ChemPubSoc Europe
DOI: 10.1002/chem.201502892
CHEMISTRY
A European Journal
Full Paper

Heterometallic Cages |*Hot Paper*|

A $\{Nb_6P_2W_{12}\}$-Based Hexameric Manganese Cluster with Single-Molecule Magnet Properties

Dongdi Zhang,[a] Fan Cao,[b] Pengtao Ma,[a] Chao Zhang,[c] You Song,[b] Zhijie Liang,[a] Xiaojing Hu,[a] Jingping Wang,*[a] and Jingyang Niu*[a]

Abstract: By deliberately using a metastable polyanion $[(NbO_2)_6P_2W_{12}O_{56}]^{12-}$ (**1**), which was formed in situ, we have discovered the unprecedented hexameric cluster $\{Mn_{15}(Nb_6P_2W_{12}O_{62})_6\}$ (**2**), in which the six polyanions $[Nb_6P_2W_{12}O_{61}]^{10-}$ are alternately connected by four intriguing trinuclear $\{Mn^{III}_3\}$ moieties and four $\{Mn^{II}\}$ linkers. This discovery is the first in which the phosphoniobotungstate has been made accessible by using transition-metal ions; furthermore, polyanion **2** represents the largest niobotungstate cluster reported to date. Analysis by means of electrospray ionization mass spectrometry (ESI-MS) provides insight into the self-assembly process, and the peaks observed relate to the different charge states of the parent cluster, thus confirming the stability of **2**. In addition, magnetic-susceptibility measurements reveal that each $\{Mn^{III}_3\}$ subunit is a separate single-molecule magnet (SMM). This discovery results from the exploration of the reverse effect of metastable polyanion **1** possessing high reactivity, thereby turning a disadvantage into an advantage. This finding could define a new synthetic strategy for the design and synthesis of magnetic polyoxometalate (POM) clusters.

Introduction

Polyoxometalates (POMs) are a unique class of metal–oxygen cluster with enormous structural diversity and various potential applications in catalysis, magnetism, medicine, and materials science.[1–3] Amongst the vast POM family, transition-metal-substituted POMs (TMSPs) are the most explored subset owing to well-established synthetic strategies, which utilize various lacunary POM species as secondary building units to construct unique clusters with a rich array of properties.[4] However, it remains a challenge to control the assembly based on preformed lacunary precursors that are known to reorganize in solution, thus greatly increasing the unpredictability of the resulting final architecture and obstructing our capacity to understand the reorganization.[5]

To date, the synthesis and characterization of saturated POM-based TMSPs remains relatively underexplored, particularly relative to the many lacunary POM-containing species. This deficiency is because the charge density of a saturated polyoxotungstate (POT) is too diffuse for the oxo ligands to be nucleophilic enough, therefore these ligands remain mostly unreactive toward electrophiles.[6] However, the introduction of substituents into the polyoxometallic framework, notably the addendum metal atom in an oxidation state lower than six, will increase the nucleophilicity of the oxo ligands, which is an attractive way to cover this lack of selectivity. In this context, the Nb/W addendum clusters, which were first reported in 1976 by Dabbabi and Boyer,[7] represent one of the largest subsets in mixed-addenda POM chemistry. However, to date, most of the reported studies are still dominated by Lindqvist-type-supported organometallic derivatives[8] and Keggin-type oligomeric clusters.[9–10] To the best of our knowledge, the largest Keggin-type niobotungstate is the tetrameric $[Nb_4O_6(XW_9Nb_3O_{40})_4]^{n-}$ ion (X = Si/Ge, $n = 20$; X = As, $n = 16$), in which each of the four $\{XW_9Nb_3O_{40}\}$ Keggin units is connected by three Nb-O-Nb bridges to the $\{Nb_4O_6\}$ core.[10]

It is noteworthy that the monomeric Wells–Dawson-type $[(NbO_2)_6P_2W_{12}O_{56}]^{12-}$ ion ($\{(NbO_2)_6P_2W_{12}\}$ (**1**)), first reported by Hill and co-workers as early as 1997, has received little attention probably owing to its instability.[11] By utilizing $\{(NbO_2)_6P_2W_{12}\}$ formed in situ instead of isolation, our group has just recently reported several oligomeric Wells–Dawson-type-based Nb/W assemblies, that is, $\{(P_2W_{12}Nb_6)_2\}$, $\{(Nb_4O_6)(P_2W_{12}Nb_6)_4\}$, and $\{(Nb_4O_6)(P_2W_{12}Nb_7)_4\}$, in which the $\{Nb_6P_2W_{12}\}$ structure can be well stabilized as a dimer or tetramer.[12] These structures emphasize that the template effect may play an important role during the formation of these assemblies. It has been thoroughly demonstrated that the NbO_2 groups in polyanion **1** are actually more basic and reactive

---

[a] Dr. D. Zhang, P. Ma, Z. Liang, X. Hu, Prof. J. Wang, Prof. Dr. J. Niu
Henan Key Laboratory of Polyoxometalate Chemistry
College of Chemistry and Chemical Engineering
Henan University, Kaifeng 475004 (P.R. China)
E-mail: niujy@henu.edu.cn
wjp@henu.edu.cn

[b] F. Cao, Prof. Dr. Y. Song
State Key Laboratory of Coordination Chemistry
Nanjing University, Nanjing 210093 (P.R. China)

[c] C. Zhang
Collaborative Innovation Center of Chemistry for Energy Materials
Xiamen University, Xiamen 361005 (P.R. China)

Supporting information for this article is available on the WWW under http://dx.doi.org/10.1002/chem.201502892.

than their oxotungsten counterparts. Therefore, $\{(NbO_2)_6P_2W_{12}\}$ formed in situ can indeed be regarded as a saturated building block to generate gigantic POM assemblies. In this way, it is possible to fill in the gaps in the Nb/W-based TMSPs by using a $\{(NbO_2)_6P_2W_{12}\}$ fragment as an inorganic multidentate oxygen-donor ligand to encapsulate paramagnetic metal ions, thus leading to larger clusters with interesting magnetic properties.

On the other hand, POMs show great potential as single-molecule magnets (SMMs) because they may shield the magnetic core from interaction with other molecules, thus creating a discrete magnet.[4c,13,14] The field of POM-based SMMs has been studied since the pioneering work of Cronin and co-workers showed that the mixed-valence core $[Mn^{III}_4Mn^{II}_2O_4(H_2O)_4]^{8+}$ ion can be encapsulated between two $\{XW_9O_{34}\}$ ($X = Ge^{IV}$, Si^{IV}) moieties.[14a] Since then only a small number of POM-based 3d SMMs have been described, such as two Fe^{III} complexes with hexa- and nonanuclearity $(Fe_4(FeW_9)_2\}$ and $\{(Fe_4W_9)_2(FeW_6)\}$, respectively),[14b] three Co^{II}-substituted clusters with hexadeca-, hepta-, and tetradecanuclearity $\{(Co_{16}(PW_9)_4\}$,[14c] $\{Co_7(PW_9)_2\}$,[14d] and $\{Co_{14}[P_2W_{15}]_4\}$, respectively),[14e] two $Mn^{III/IV}$ cubane complexes with tetra- and heptanuclearity ($\{(SiW_9)Mn^{III}_3Mn^{IV}\}$[14f] and $\{(P_2W_{15})_2Mn^{III}_6Mn^{IV}\}$, respectively).[14g] However, the number of POM-based SMMs is still very small relative to the hundreds of already known SMMs.

Herein, we present the unprecedented double-staggered wheel-shaped $[H_{123}Nb_{36}P_{12}W_{72}Mn^{III}_{12}Mn^{II}_3NaO_{424}]^{10-}$ ion (**2**), in the form $K_{10}\mathbf{2}\cdot 26H_2O$ (**2a**; Figure 1). To the best of our knowledge, polyanion **2** is the first example of a transition-metal-substituted derivative of a heteroniobotungstate. It is by far the highest polymerization example of its type and the largest niobotungstate cluster ever reported. More interestingly, **2a** exhibits SMM behavior with an energy barrier of 27.5(5) K, slightly higher than that of any other POM-based 3d SMMs.[14]

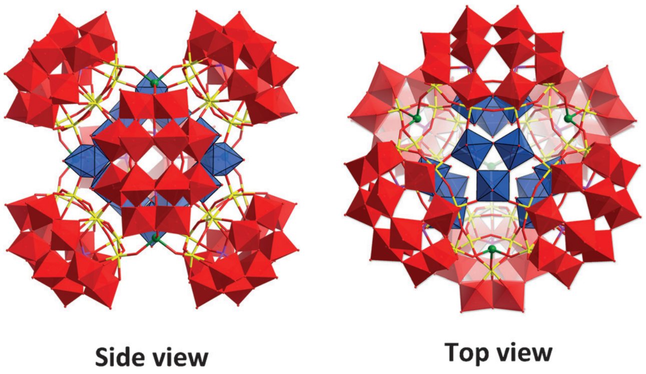
Side view
Top view

Figure 1. Representation of the double-staggered framework of polyanion **2**. The trimeric $\{Mn_3\}$ cores and $\{Mn\}$ hinges are highlighted in the blue octahedra and green spheres, respectively. The cations and solvent water molecules have been omitted for clarity. Red octahedra: WO_6; red sticks: O; pink sticks: P; yellow sticks: Nb.

Results and Discussion

Insight into the reactivity of the $\{(NbO_2)_6P_2W_{12}\}$ building block

It is well known that the α-$[H_2P_2W_{12}O_{48}]^{12-}$ ion (P_2W_{12}) is a highly lacunary ligand in which vacancies in the framework may be occupied by additional metal ions to give diverse higher-nuclearity mixed-metal clusters, especially with respect to their magnetic properties. Nevertheless, it must be realized that this metastable synthon easily undergoes structural transformations in aqueous media,[15] but it is difficult to predict which fragments will form and harder still to trap desired fragments in a final architecture. We focused our interest on the Wells–Dawson polyanion $\{(NbO_2)_6P_2W_{12}\}$ (**1**) unveiled by Hill and co-workers[11] to search for ligands that might be an appropriate precursor for paramagnetic clusters. The reason for this approach is because our recent reports have shown that the oxoniobium(V) surface of **1** is more basic and reactive than its oxotungsten(VI) counterpart.[12] If so, **1** formed in situ can be viewed as the secondary building block and serves as a likely starting point for aggregation, which could be further modified by introducing paramagnetic 3d metal ions to probe gigantic transition-metal-containing clusters and has been thoroughly demonstrated by the work presented herein.

We used electrospray ionization mass spectrometry (ESI-MS) to rationalize the molecular growth and postulate four concurrent reactions related to the formation of **2** under the selected reaction conditions:

1) The decomposition of the $[Nb_6O_{19}]^{8-}$ ion in an aqueous solution of H_2O_2, thus resulting in the release of an intermediate $\{NbO_2\}$ species.
2) The functionalization of P_2W_{12} in situ, thus giving the secondary building block $\{(NbO_2)_6P_2W_{12}\}$, which was confirmed by ESI-MS analysis. The major peaks could be satisfactorily assigned to the formula $\{(NbO_2)_6P_2W_{12}O_{56}\}$ with various combinations of K and H counterions. The observed peaks were assigned to $[K_3H_5(NbO_2)_6P_2W_{12}O_{56}]^{4-}$ and $[K_5H_4(NbO_2)_6P_2W_{12}O_{56}]^{3-}$ ions, which gave envelopes centered at *m/z* 1008.7 and 1370.7, respectively (Figure 2). Therefore, ESI-MS analysis confirmed the formation of the monomer $\{(NbO_2)_6P_2W_{12}O_{56}\}$ in situ.
3) The oxidation of the Mn^{II} species into Mn^{III} and the formation of $\{Mn^{III}_3\}$ clusters.
4) The stepwise cleavage of the O–O bonds followed by condensation to Nb-O-Mn bridges in acidic solution on heating, which stabilizes the highly charged species. Cluster **2** forms strong ionic interactions with the cations and many strong hydrogen bonds with solvent water molecules due to its high negative charge (41+) and gigantic molecular weight ($M_r > 25\,500$), thus making it harder to observe the naked single cluster without any cations and solvent molecules.[16] In the case of hexameric cluster **2**, three major peak envelopes at *m/z* 1931.9, 2099.4, and 2298.8 could be assigned to an assembly of related clusters with differing

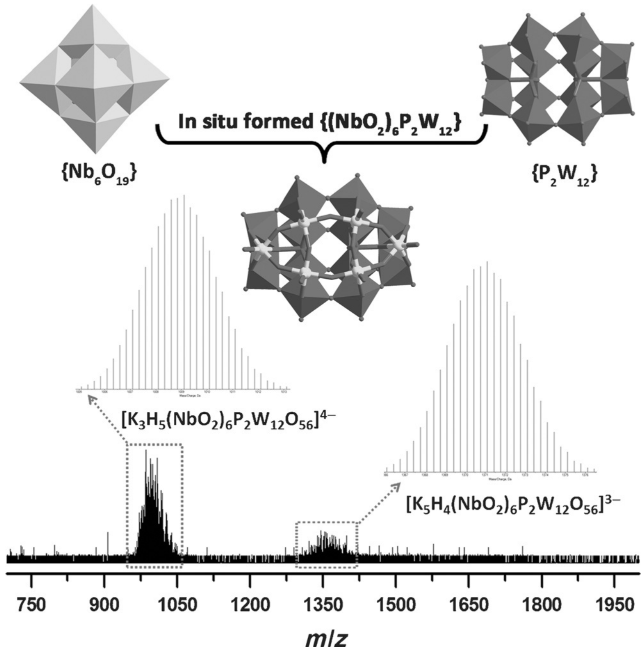

Figure 2. ESI-MS spectrum of the $\{(NbO_2)_6P_2W_{12}\}$ building block formed in situ.

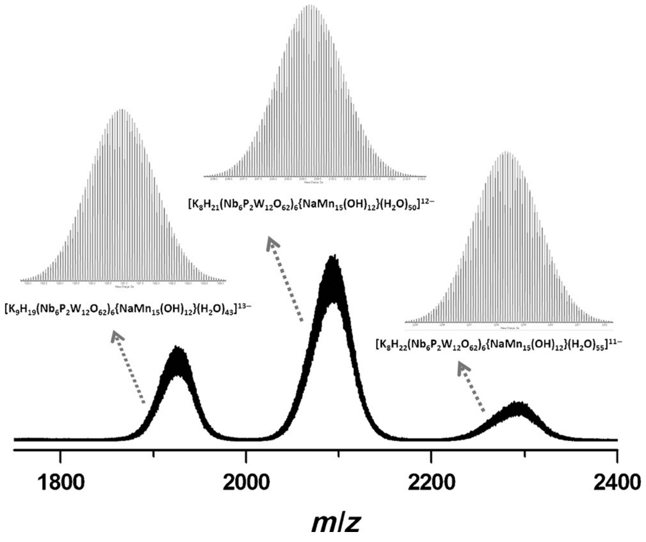

Figure 3. Negative-ion ESI mass spectrum of cluster **2**.

numbers of cations and water molecules, thus showing some degree of stability in solution (Figure 3).

Structural analysis

Single-crystal X-ray diffraction studies revealed that polyanion **2** is a unique wheel-shaped cluster that crystallizes in a monoclinic system (i.e., space group *P*2(1)*m*). The overall polyanion consists of three main parts: six peroxo-free $\{Nb_6P_2W_{12}\}$ units, four $\{Mn_3\}$ trinuclear cores, and four {Mn} hinges (see Figure S1 in the Supporting Information). It is not surprising that six niobium ions occupy the vacant sites of each hexalacunary phosphotungstate (see Figure S2 in the Supporting Information), thus confirming that $\{Nb_6P_2W_{12}\}$ can be well maintained and employed as a secondary building block. Each $\{Nb_6P_2W_{12}\}$ unit is linked to two $\{Mn_3\}$ cores and two {Mn} moieties by six Nb-O-Mn bridges (see Figure S3 in the Supporting Information), thus resulting in a giant hexamer (Figure 4). This observation is the first hexameric structure in niobotungstate chemistry, although there are many examples of dimeric and tetrameric aggregates.[10,12]

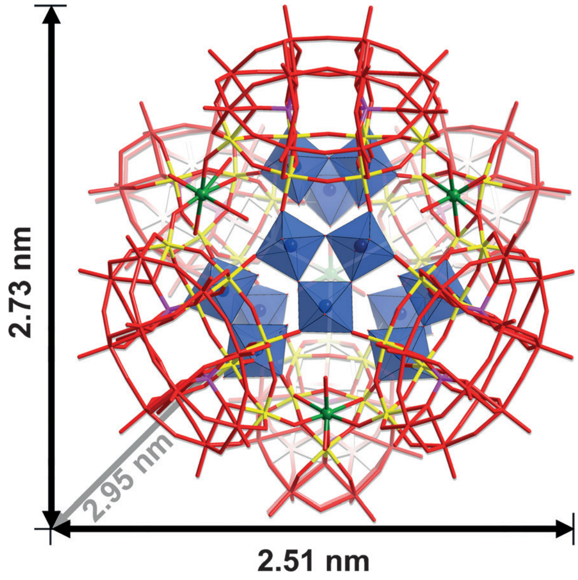

Figure 4. Representation of polyanion **2**. The cations and solvent water molecules have been omitted for clarity. The cluster measures 2.95 nm at its longest point. See Figure 1 for the labeling scheme.

The structure of $\{Mn_3\}$ is shown in Figure S4 in the Supporting Information. This species can be regarded as a group of three mutually corner-coupled $\{MnO_6\}$ octahedra. Interestingly, two of the Mn⋯Mn distances in the trinuclear $\{Mn_3\}$ unit are identical, which is slightly longer or shorter than the third Mn⋯Mn distance. Therefore, the overall shape of the $\{Mn_3\}$ unit can be described as an equivalent isosceles triangle. Each $\{Mn_3\}$ unit is surrounded by three Well–Dawson $\{Nb_6P_2W_{12}\}$ units and six Mn-O-Nb bridges (Figure 5 a). All the Mn ions in

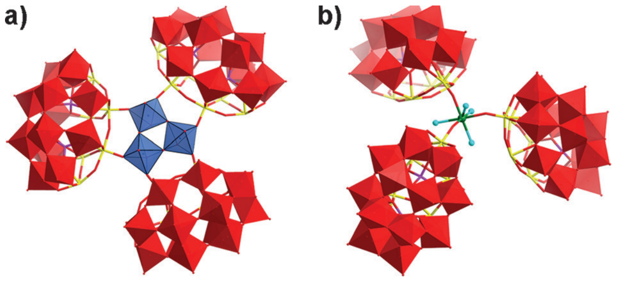

Figure 5. a) Representation of the $[Mn^{III}_3(OH)_3(H_2O)_6]^{6+}$ core, b) $\{Mn_3\}$ core, and c) {Mn} moiety within **2**.

these moieties are in the +3 valence state, as established by a combination of bond-valence sum (BVS) calculations[17] (see Table S1 in the Supporting Information) and the characteristic Jahn–Teller distortion for Mn^{III} (high-spin d^4; see Figure S5 in the Supporting Information). The BVS calculations indicate the presence of three monoprotonated oxygen atoms (μ_2-bridging OH group) and six terminal diprotonated oxygen atoms in the trimeric manganese core of polyanion **2** (see Figure S6 in the Supporting Information), thus resulting in a $[Mn^{III}_3(OH)_3(H_2O)_6]^{6+}$ core.

Each {Mn} hinge shows crystallographic positional disorder of Mn^{II} and Na (0.75:0.25). Each of the four Mn^{II}/Na centers is coordinated by three μ_2-oxo groups and four terminal oxygen atoms, thus leading to a distorted single-crown octahedral geometry (Figure 5b). The BVS calculations confirm that the four terminal oxygen atoms are all diprotonated (see Figure S6 in the Supporting Information). Therefore, this disordered metal center should be formulated as $[Mn^{II}_{0.75}Na_{0.25}(H_2O)_4]^{1.75+}$. In Table S2 (see the Supporting Information), the BVS values for all the oxygen atoms in **2** are also listed. The BVS values for mono- and diprotonated oxygen atoms were 1.30–1.40 and 0.25–0.61, respectively. In addition, charge-balance considerations with the countercations suggested that **2a** contains some protons, namely, $K_{10}[H_{31}(Nb_6P_2W_{12}O_{62})_6\{Mn^{III}_3(OH)_3(H_2O)_6\}_4\{Mn^{II}_{0.75}Na_{0.25}(H_2O)_4\}_4]\cdot 26\,H_2O$. As was stated already by Nyman and co-workers and us,[18] the very large number of crystallographically independent atoms and parameters prevented the direct location of protons from the Fourier maps. Thus, we think that thirty-one protons are probably delocalized in polyanion **2**.

Alternatively, **2** can be viewed as six P_2W_{12} fragments that support an unprecedented $\{Nb_{36}Mn_{15}Na\}$ cluster (see Figure 6 and Figure S7 in the Supporting Information), which is the largest 3d–4d heterometallic array in POM chemistry. The cluster described here presents new interesting and unusual features. First, the $\{Nb_{36}Mn_{15}Na\}$ cluster is the first example of a Mn/Nb-core-based POM. Second, the plenary polyanion **1**, like the classic lacunary POMs, displays a tendency to incorporate transition-metal centers, thus constructing a new type of TMSP family. In addition, to the best of our knowledge, polyanion **2** represents the largest aggregate of Nb-substituted POMs and the first example of a phosphoniobotungstate-based transition-metal derivative.

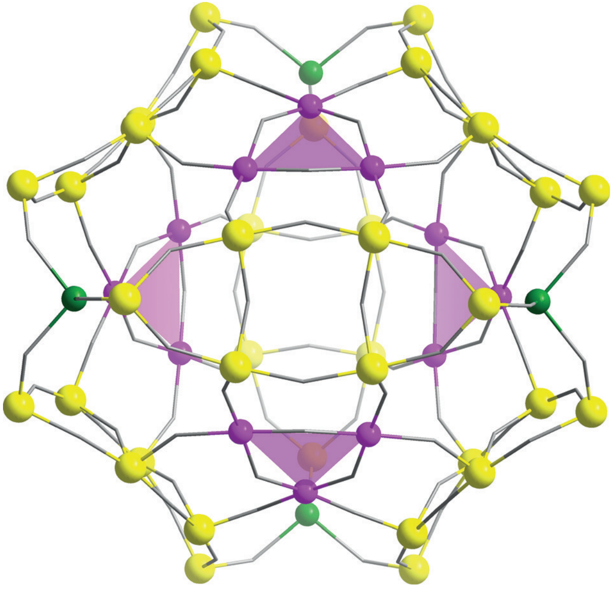

Figure 6. Ball-and-stick representation of the $\{Nb_{36}Mn_{15}Na\}$ cluster in **2**. Nb: yellow, Mn^{III}: pink, Mn^{II}/Na: green, O: gray.

As mentioned above, the starting material P_2W_{12} is a metastable precursor that could easily undergo structural transformations in aqueous media;[15] hence, only very few polyanions are known in which the hexalacunary P_2W_{12} fragment is maintained in the product.[11,12,19–21] In recent years, P_2W_{12} has been utilized in the assembly of larger dimeric,[12b,19] trimeric,[20] and tetrameric[21] aggregates arranged as open or crown-type structures (Figure 7), but a higher polymeric complex based on P_2W_{12} has not yet been observed. Notably, hexameric **2** has retained this entity. The only known hexamric Well–Dawson-type structure is the $[\{\alpha\text{-}P_2W_{15}O_{56}\}_6\{Ce_3Mn_2O_4(OH)_2\}_3(OH)_2(H_2O)_2(PO_4)]^{47-}$ ion (**3**) reported by Fang and Kögerler in 2008.[22] Polyanion **3** is based on trilacunary $[P_2W_{15}O_{56}]^{12-}$ (P_2W_{15}) instead of the hexalacunary P_2W_{12} fragment in **2**. The difference between **2** and **3** is that there are six P_2W_{12} subunits in **2** linked by 36 $Mn^{II/III}$-O-Nb bridges involving six crescent shape $\{Nb_6\}$ clusters, four triangle $\{Mn_3\}$ cores, and four {Mn} moieties, whereas there are six P_2W_{15} units in **3** interconnected by three $\{Ce_3Mn_2\}$ cores and a central PO_4^{3-} group. Compound **2** represents the first example of a P_2W_{12}-based hexamer.

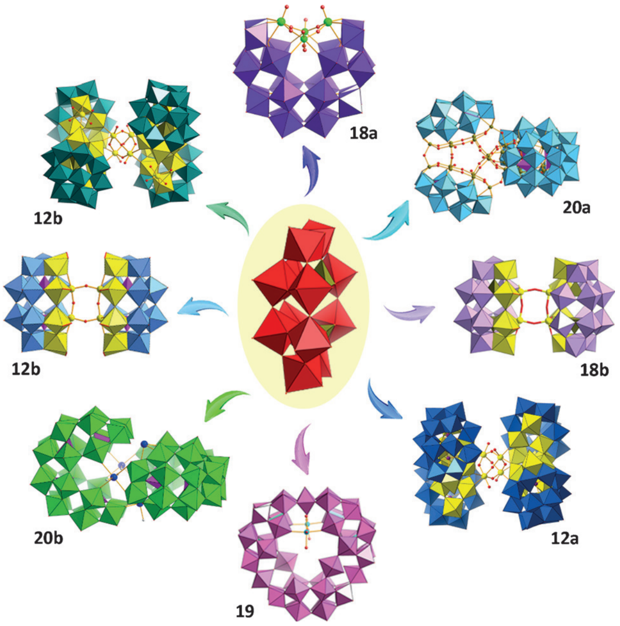

Figure 7. Reported POMs, in which the structure of the P_2W_{12} precursor has been maintained.

Magnetic studies

Due to the presence of the four triangles in **2a**, it was expected that these compounds might be magnetically interesting as SMMs;[23] hence, the magnetic properties of **2a** were studied. Variable-temperature direct-current (dc) magnetic-susceptibility (χ_M) studies were performed on dried crystalline samples of **2a** in the temperature range 1.8–300 K in an applied field of 2 kOe. The results are presented as plots of $\chi_M T$ versus T in Figure 8.

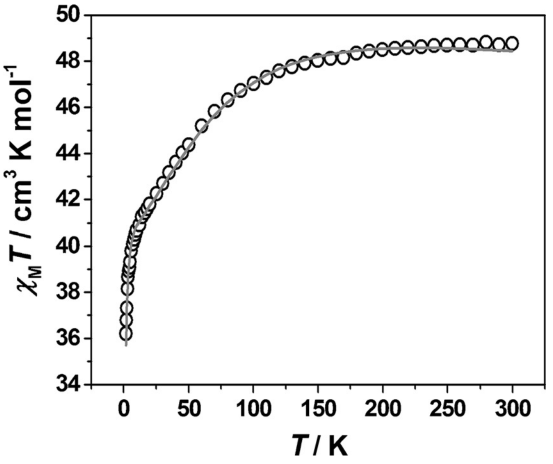

Figure 8. Temperature dependence of the magnetic properties of **2a** at 2 kOe. The solid line is the best fit obtained by using the Hamiltonian magnetic model described in the text.

At room temperature, the $\chi_M T$ product is 48.75 cm^3 K mol^{-1}, close to the spin-only value ($g=2$) of 49.125 cm^3 K mol^{-1} expected for three Mn^{II} ions ($S_{Mn^{II}}=5/2$) and twelve Mn^{III} ions ($S_{Mn^{III}}=2$). Upon cooling, the $\chi_M T$ products steadily decrease until 40 cm^3 K mol^{-1} at 5 K, before sharply dropping to reach 35.7 cm^3 K mol^{-1} at 1.8 K. This thermal behavior is diagnostic of dominant antiferromagnetic interactions within the cluster. The observed change of $\chi_M T$ at 5 K is suggested to correspond to the ground-state spin. According to the structure of **2a**, we can consider that all the Mn^{II} ions and {Mn$^{III}_3$} units may be magnetically isolated, such that the ground-state spin of a trinuclear species can be estimated to be $S_T=3$ (calculated $\chi_M T = 0.125\times g^2\times[3S_{Mn^{II}}(S_{Mn^{II}}+1)+4S_T(S_T+1)]=37.125$ cm^3 K mol^{-1}). This spin value possibly comes from the frustrated geometrical configuration of the {Mn$^{III}_3$} triangle.

The PHI program[24] was used to fit the variable-temperature magnetic properties and determine coupling between the Mn^{III} ions and the ground-state spin. Inspection of the molecular structure reveals that all the {Mn$^{III}_3$} units can be approximately regarded as equivalent isosceles triangle with two coupling constants. Therefore, only one {Mn$^{III}_3$} cluster ($(\chi_M T_{obs}-3C_{Mn^{II}})/4$, in which $C_{Mn^{II}}$ is the Curie constant of the Mn^{II} ion) was fitted with the following Hamiltonian in Equation (1):

$$H = -2J(S_A S_B + S_A S_C) - 2J' S_B S_C \quad (1)$$

The best fitting results gave $J=19.98$ cm^{-1}, $J'=-20.49$ cm^{-1}, and $g=1.87$ with $R=0.12$ (solid line in Figure 8). The (F, AF) combination may lead to spin frustration and involve an intermediate spin ground-state value $S=3$ deduced from the experimental data. The ratio $J/J'=19.98/-20.49=-0.98$ is in good agreement with the prediction from the energy-distribution plots with the ratio between approximately -1.0 to -0.5, thus corresponding to a $|3,1>$ ground state (Figure 9). A similar special magnetic phenomenon was observed in a {Mn$^{III}_3$} triangle topology system with $J/J'=40.5/-10.8=3.75$.[23a]

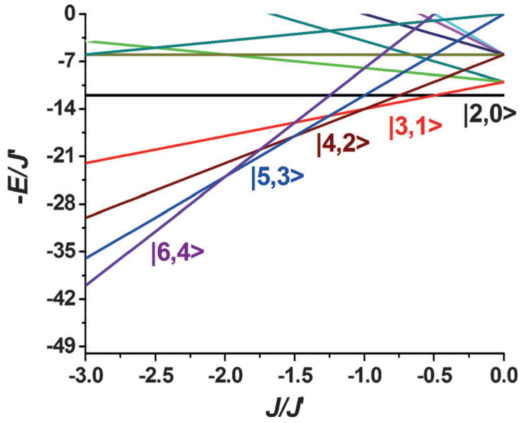

Figure 9. Energy-distribution plots of **2a** with a ratio of J/J' for the (F, AF) combination of J and J'. The ground states are labeled as $|S_T, S_{BC}>$, in which $S_{BC}=S_B+S_C$ and $S_T=S_{BC}+S_A$.

The variable-field magnetization was measured in an applied field of 0–70 kOe at 1.8 K to confirm the ground-state spin (see Figure S8 in the Supporting Information). In the low fields, the magnetization increases quickly and slowly before and after 20 kOe, respectively. The maximum magnetization is 42.5 $N\mu_B$ in 70 kOe, which is higher than the calculated value of 37.44 $N\mu_B$ ($\Sigma gS = 2\times5/2\times3+1.87\times3\times4$), thus indicating that the population changed in high fields for {Mn$^{III}_3$}. The Zeeman-splitting energy-distribution plots were simulated by using the PHI program[24] (Figure 10), from which it is easy to find that the ground-state spin is field dependent. The ground state is $|3,1>$ when the field ranges from 0 to 2.3 T, at which point $|4,2>$ becomes the ground state in high fields. So, the plot of M versus H shows a linear increase in a high-field region without clear saturation at 7 T. According to $S_T=4$ of {Mn$^{III}_3$}, the saturation magnetization is estimated to be 45 $N\mu_B$ for **2a**.

The variable-temperature isofield magnetization was also measured. The isofield lines of reduced magnetization, that is, M versus H/T, for **2a** do not superimpose (Figure 11), thus indicating significant magnetic anisotropy in the ground state for the {Mn$^{III}_3$} units. This finding urged us to investigate the possible SMM properties of **2a**.

The variable-temperature alternating-current (ac) signals showed strong frequency dependence both in- and out-of-phase (see Figure S9 in the Supporting Information). In the ac susceptibilities of the in-phase, there no obvious peak was observed and χ_M' increases with cooling. This phenomenon indi-

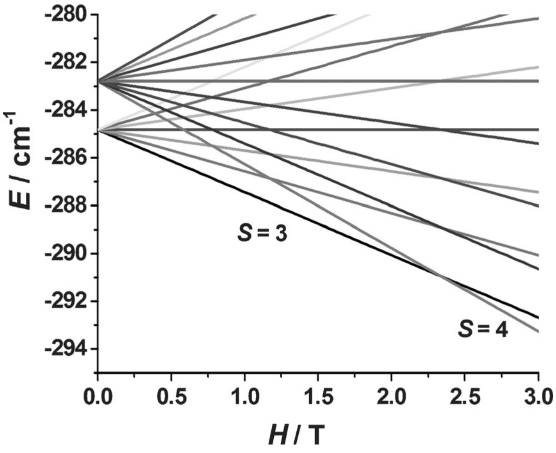

Figure 10. Zeeman splitting of the lowest m_s states of {Mn^{III}_3} for the lowest total spin state from 0 to 7 T.

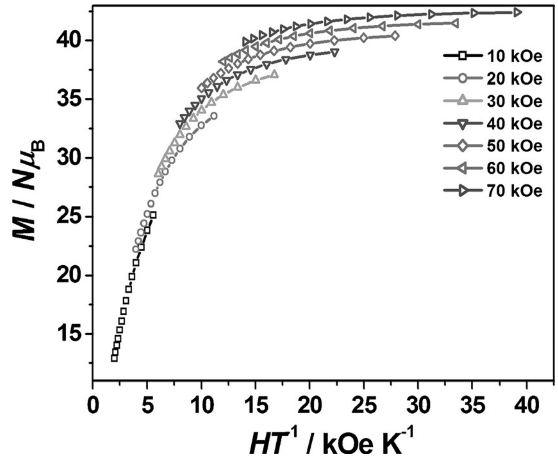

Figure 11. Plots of M versus H/T of **2a**.

cates the coexistence of paramagnetic and superparamagnetic phases, which can be ascribed to the contributions of noninteracting Mn^{II} ions and {Mn^{III}_3} units. A typical curve with the coexistence of two phases usually resembles a lying down "S". The variable-frequency ac curves are shown in Figure 12. In the isotemperature curves, the peak frequencies were chosen to illustrate the ln(τ) versus 1/T plot, which is in a good agreement with the Arrhénius law $\tau(T) = \tau_0\exp(\Delta E/k_BT$; see Figure S10 in the Supporting Information). The fitting results gave the relaxation time $\tau_0 = 1.2(3)\times10^{-11}$ s and the energy barrier $\Delta E/k_B =$ 27.5(5) K, which are consistent with SMM behavior and suggested from the {Mn^{III}_3} units. At fixed temperatures from 1.8 to 2.4 K, incomplete semicircle Cole–Cole curves were obtained (Figure 13), which were fitted by using a generalized Debye model.[25] The obtained α parameters are 0.38–0.61, thus indicating a large distribution of relaxation time, which can possibly be attributed to the difference in the magnetic properties of the four {Mn^{III}_3} units.

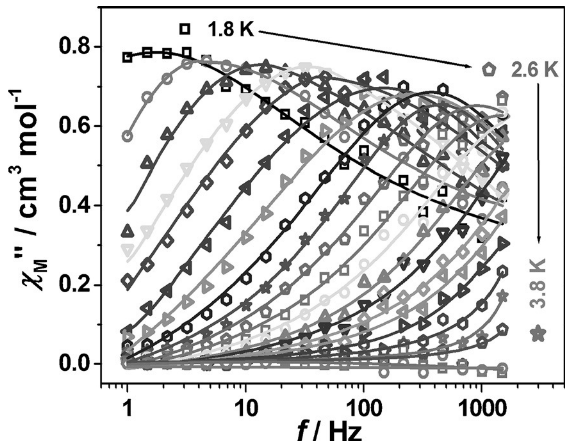

Figure 12. Frequency dependence of out-of-phase susceptibilities of **2a** with $H_{dc} = 0$, $H_{ac} = 5$ Oe, and $f = 1$–1488 Hz in range $T = 1.8$–5 K.

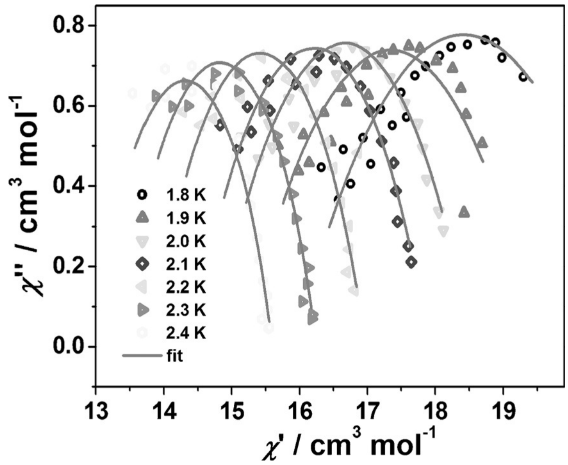

Figure 13. The solid line represents the least-squares fit of the experimental data to the Arrhénius equation for **2a**.

Conclusion

An unprecedented hexameric POM cluster has been successfully obtained by utilizing the saturated Wells–Dawson-type {$(NbO_2)_6P_2W_{12}$} unit, which was formed in situ, as the secondary building block. Compound **2a** is a very rare example of a hexameric POM, which represents the first example of a {$Nb_6P_2W_{12}$}-based manganese complex with SMM behavior and contains the largest {$Nb_{36}Mn_{15}Na$} heterometallic array in POM chemistry. Furthermore, **2a** behaves as a SMM with an energy barrier of 27.5(5) K, slightly higher than that of any other POM-based 3d SMMs. The formation of polyanion **2** exemplifies the reactivity of {$(NbO_2)_6P_2W_{12}$} with manganese metal ions, thereby turning a disadvantage into an advantage and providing an alternative perspective for the construction of novel TMSP architectures with intriguing properties. In further work, we will extend this approach with paramagnetic transition-metal species because we believe such clusters will also show novel properties.

Experimental Section

Materials and methods

General: All the reagents and solvents were purchased from commercial suppliers and used as received. $K_7[HNb_6O_{19}]\cdot 13\,H_2O$and $K_{12}[H_2P_2W_{12}O_{48}]\cdot 24\,H_2O$ were synthesized according to a reported procedure.[26] IR spectra ($\tilde{\nu} = 4000–400\ cm^{-1}$) of the samples were recorded on an AVATAR360 FTIR spectrometer. Elemental analyses (Mn, Nb, and W) were obtained on a PerkinElmer Optima 2100 DV by using inductively coupled plasma optical emission spectrometry.

Preparation of 2a: $K_7[HNb_6O_{19}]\cdot 13\,H_2O$ (1.60 g, 1.17 mmol) was dissolved in a solution of H_2O_2 (13.5 mL, 30 %) in water (165 mL). Diluted hydrochloric acid (1 M, 12.5 mL) was added dropwise and then powdered $K_{12}[H_2P_2W_{12}O_{48}]\cdot 24\,H_2O$ (4.65 g, 1.18 mmol) was added in a single step to the reaction mixture with rapid stirring to give a clear yellow solution. The solution was adjusted to approximately pH 2.0 by the addition of aqueous HCl (0.5 M). The suspension was continuously stirred for approximately 1 h and then filtered to obtain a clear solution. A solution of $MnCl_2\cdot 4\,H_2O$ (2.32 g, 11.7 mmol) in H_2O (30 mL) was added with stirring. The solution was adjusted to pH 2.4 and heated to 90 °C for 10 h. The reaction mixture was removed from the hot plate and left to cool to room temperature, followed by the addition of KCl (2.65 g, 35.6 mmol). The reaction mixture was stirred for 30 min and filtered. The clear dark-purple filtrate was kept in an open beaker at room temperature to allow slow evaporation. Subsequent crystallization over one month yielded a dark-purple hydrated salt in 12 % yield (based on Nb). IR: $\tilde{\nu} = 3430$(s), 1624 (s), 1094 (s), 1056 (w), 1006 (w), 956 (s), 900 (m), 784(s), 674 cm^{-1} (m); elemental analysis (%) calcd for $M_w = 25\,566.9$: Mn 3.22, Nb 13.08, W 51.77; found: Mn 3.34, Nb 12.42, W 50.28.

X-ray crystal-structure analyses

Suitable single crystals were selected from their respective mother liquors and placed in a thin glass tube due to efflorescence. X-ray diffraction intensity was recorded on a Bruker Apex-II CCD diffractometer at 296(2) K with MoKα monochromated radiation ($\lambda = 0.71073$ Å). Structure solution and refinement were carried out by using the SHELXS-97 and SHELXL-97 program package.[27] No hydrogen atoms were located from the difference Fourier map. Further details of the crystal structure investigation can be obtained from the Fachinformationszentrum Karlsruhe, 76344 Eggenstein-Leopoldshafen, Germany (fax: (+49)7247–808–666; e-mail: crysdata@fiz-karlsruhe.de) on quoting the depository number CSD-429760.

Magnetic measurements

Magnetic-susceptibility data of **2a** ($m = 57.48$ mg) were recorded on a Quantum Design SQUID magnetometer in fields up to 7 T between 1.8 and 300 K. The temperature and frequency dependent ac susceptibility measurements in different applied static magnetic fields were carried out in an oscillating ac field of 5.0 Oe and frequencies of 1–1500 Hz. The magnetic-susceptibilities data were corrected for the sample holder and the diamagnetism of the constituent atoms (estimated byb using the Pascal constants).

ES-MS measurements

ESI-MS measurements were carried out at 30 °C. The solution of the sample was diluted so that the maximum concentration of the cluster ion was on the order of 10^{-5} M, which was infused at a flow rate of 10 μL min^{-1}. The measurements were carried out on a AB SCIEXTriple TOF 4600 mass spectrometer, and the data were collected in the negative mode.

Acknowledgements

This work was supported by the National Natural Science Foundation of China (grant numbers 91222102, 21171089, and 21371048), Major State Basic Research Development Program (2013CB922102), the NSF from Henan Province (grant number 142300410009), and Henan University.

Keywords: heterometallic cages · magnetic properties · molecular magnetism · polyoxometalates · transition metals

[1] a) M. T. Pope, A. Müller, *Angew. Chem. Int. Ed. Engl.* **1991**, *30*, 34–48; *Angew. Chem.* **1991**, *103*, 56–70; b) D.-L. Long, R. Tsunashima, L. Cronin, *Angew. Chem.* **2010**, *122*, 1780–1803; *Angew. Chem.* **2010**, *122*, 1780–1803.

[2] a) Y. Wang, I. A. Weinstock, *Chem. Soc. Rev.* **2012**, *41*, 7479–7496; b) H. Lv, Y. V. Geletii, C. Zhao, J. W. Vickers, G. Zhu, Z. Luo, J. Song, T. Lian, D. G. Musaev, C. L. Hill, *Chem. Soc. Rev.* **2012**, *41*, 7572–7598; c) A. Proust, B. Matt, R. Villanneau, G. Guillemot, P. Gouzerh, G. Izzet, *Chem. Soc. Rev.* **2012**, *41*, 7605–7622.

[3] a) T. Liu, M. L. K. Langston, J. M. Pigga, C. Pichon, A. M. Todea, A. Müller, *Science* **2011**, *331*, 1590–1592; b) D.-Y. Du, L.-K. Yan, Z.-M. Su, S.-L. Li, Y.-Q. Lan, E.-B. Wang, *Coord. Chem. Rev.* **2013**, *257*, 702–717; c) B. Rausch, M. D. Symes, G. Chisholm, L. Cronin, *Science* **2014**, *345*, 1326–1330.

[4] a) A. Dolbecq, E. Dumas, C. R. Mayer, P. Mialane, *Chem. Rev.* **2010**, *110*, 6009–6048; b) O. Oms, A. Dolbecq, P. Mialane, *Chem. Soc. Rev.* **2012**, *41*, 7497–7536; c) J. M. Clemente-Juan, E. Coronado, A. Gaita-Ariño, *Chem. Soc. Rev.* **2012**, *41*, 7464–7478; d) S.-T. Zheng, G.-Y. Yang, *Chem. Soc. Rev.* **2012**, *41*, 7623–7646; e) M. Ibrahim, Y. X. Xiang, B. S. Bassil, Y. H. Lan, A. K. Powell, P. Oliveira, B. Keita, U. Kortz, *Inorg. Chem.* **2013**, *52*, 8399–8408; f) R. S. Winter, J. M. Cameron, L. Cronin, *J. Am. Chem. Soc.* **2014**, *136*, 12753–12761.

[5] a) S. G. Mitchell, P. I. Molina, S. Khanra, H. N. Miras, A. Prescimone, G. J. T. Cooper, R. S. Winter, E. K. Brechin, D.-L. Long, R. J. Cogdell, L. Cronin, *Angew. Chem. Int. Ed.* **2011**, *50*, 9154–9157; *Angew. Chem.* **2011**, *123*, 9320–9323; b) R. S. Winter, J. Yan, C. Busche, J. S. Mathieson, A. Prescimone, E. K. Brechin, D.-L. Long, L. Cronin, *Chem. Eur. J.* **2013**, *19*, 2976–2981; c) L. Huang, S. S. Wang, J.-W. Zhao, L. Cheng, G.-Y. Yang, *J. Am. Chem. Soc.* **2014**, *136*, 7637–7642.

[6] a) W. Knoth, R. Harlow, *J. Am. Chem. Soc.* **1981**, *103*, 4265–4266; b) V. W. Day, W. G. Klemperer, C. Schwartz, *J. Am. Chem. Soc.* **1987**, *109*, 6030–6044.

[7] M. Dabbabi, M. Boyer, *J. Inorg. Nucl. Chem.* **1976**, *38*, 1011–1014.

[8] a) C. J. Besecker, W. G. Klemperer, *J. Am. Chem. Soc.* **1980**, *102*, 7598–7600; b) C. J. Besecker, W. G. Klemperer, V. W. Day, *J. Am. Chem. Soc.* **1982**, *104*, 6158–6159; c) W. G. Klemperer, V. W. Day, *Science* **1985**, *228*, 533–541; d) V. W. Day, W. G. Klemperer, D. J. Main, *Inorg. Chem.* **1990**, *29*, 2345–2355; e) W. G. Klemperer, D. J. Main, *Inorg. Chem.* **1990**, *29*, 2355–2360; f) F. Bannani, R. Thouvenot, M. Dabbabi, *Eur. J. Inorg. Chem.* **2007**, 4357–4363.

[9] a) R. G. Finke, M. W. Droege, *J. Am. Chem. Soc.* **1984**, *106*, 7274–7277; b) M. K. Harrup, G.-S. Kim, H. Zeng, R. P. Johnson, D. VanDerveer, C. L. Hill, *Inorg. Chem.* **1998**, *37*, 5550–5556; c) G.-S. Kim, H. D. Zeng, J. T. Rhule, I. A. Weinstock, C. L. Hill, *Chem. Commun.* **1999**, 1651–1652; d) G.-S. Kim, H. Zeng, W. A. Neiwert, J. J. Cowan, D. VanDerveer, C. L. Hill, I. A. Weinstock, *Inorg. Chem.* **2003**, *42*, 5537–5544.

[10] a) G.-S. Kim, H. Zeng, D. VanDerveer, C. L. Hill, *Angew. Chem. Int. Ed.* **1999**, *38*, 3205–3207; *Angew. Chem.* **1999**, *111*, 3413–3416; b) S. J. Li, S. X. Liu, C. C. Li, F. J. Ma, D. D. Liang, W. Zhang, R. K. Tan, Y. Y. Zhang, L. Xu, *Chem. Eur. J.* **2010**, *16*, 13435–13442; c) S. J. Li, S. X. Liu, C. C. Li, F. J.

Ma, W. Zhang, D. D. Liang, R. K. Tan, Y. Y. Zhang, Q. Tang, *Inorg. Chim. Acta* **2011**, *376*, 296 – 301.

[11] D. A. Judd, Q. Chen, C. F. Campana, C. L. Hill, *J. Am. Chem. Soc.* **1997**, *119*, 5461 – 5462.

[12] a) D. Zhang, Z. Liang, S. Xie, P. Ma, C. Zhang, J. Wang, J. Niu, *Inorg. Chem.* **2014**, *53*, 9917 – 9922; b) D. Zhang, C. Zhang, P. Ma, R. Al-Oweini, B. S. Bassil, U. Kortz, J. Wang, J. Niu, *Inorg. Chem. Front.* **2015**, *2*, 254 – 262.

[13] M. A. AlDamen, J. M. Clemente-Juan, E. Coronado, C. Martí-Gastaldo, A. Gaita-Ariño, *J. Am. Chem. Soc.* **2008**, *130*, 8874 – 8875.

[14] a) C. Ritchie, A. Ferguson, H. Nojiri, H. N. Miras, Y.-F. Song, D.-L. Long, E. Burkholder, M. Murrie, P. Kögerler, E. K. Brechin, L. Cronin, *Angew. Chem. Int. Ed.* **2008**, *47*, 5609 – 5612; *Angew. Chem.* **2008**, *120*, 5691 – 5694; b) J.-D. Compain, P. Mialane, A. Dolbecq, I. M. Mbomekallé, J. Marrot, F. Sécheresse, E. Rivière, G. Rogez, W. Wernsdorfer, *Angew. Chem. Int. Ed.* **2009**, *48*, 3077 – 3081; *Angew. Chem.* **2009**, *121*, 3123 – 3127; c) M. Ibrahim, Y. Lan, B. S. Bassil, Y. Xiang, A. Suchopar, A. K. Powell, U. Kortz, *Angew. Chem. Int. Ed.* **2011**, *50*, 4708 – 4711; *Angew. Chem.* **2011**, *123*, 4805 – 4808; d) H. El Moll, A. Dolbecq, J. Marrot, G. Rousseau, M. Haouas, F. Taulelle, G. Rogez, W. Wernsdorfer, B. Keita, P. Mialane, *Chem. Eur. J.* **2012**, *18*, 3845 – 3849; e) C. Lydon, M. M. Sabi, M. D. Symes, D.-L. Long, M. Murrie, S. Yoshii, H. Nojiri, L. Cronin, *Chem. Commun.* **2012**, *48*, 9819 – 9821; f) X. Fang, K. McCallum, H. D. Pratt III, T. M. Anderson, K. Dennis, M. Luban, *Dalton Trans.* **2012**, *41*, 9867 – 9870; g) X. Fang, P. Kögerler, M. Speldrich, H. Schilder, M. Luban, *Chem. Commun.* **2012**, *48*, 1218 – 1220.

[15] a) B. Godin, J. Vaissermann, P. Herson, L. Ruhlmann, M. Verdaguer, P. Gouzerh, *Chem. Commun.* **2005**, 5624 – 5626; b) Y.-W. Li, Y.-G. Li, Y.-H. Wang, X.-J. Feng, Y. Lu, E.-B. Wang, *Inorg. Chem.* **2009**, *48*, 6452 – 6458; c) X. Fang, P. Kögerler, Y. Furukawa, M. Speldrich, M. Luban, *Angew. Chem. Int. Ed.* **2011**, *50*, 5212 – 5216; *Angew. Chem.* **2011**, *123*, 5318 – 5322.

[16] J. Gao, J. Yan, S. Beeg, D.-L. Long, L. Cronin, *J. Am. Chem. Soc.* **2013**, *135*, 1796 – 1805.

[17] D. Altermatt, I. D. Brown, *Acta Crystallogr. Sect. B.* **1985**, *41*, 244 – 247.

[18] a) R. P. Bontchev, M. Nyman, *Angew. Chem. Int. Ed.* **2006**, *45*, 6670 – 6672; *Angew. Chem.* **2006**, *118*, 6822 – 6824; b) J. Niu, P. Ma, H. Niu, J. Li, J. Zhao, Y. Song, J. Wang, *Chem. Eur. J.* **2007**, *13*, 8739 – 8748.

[19] a) Z.-M. Zhang, S. Yao, Y.-F. Qi, Y.-G. Li, Y.-H. Wang, E.-B. Wang, *Dalton Trans.* **2008**, 3051 – 3053; b) Y. Ren, Y. Hu, Y. Shan, Z. Kong, M. Gu, B. Yue, H. He, *Inorg. Chem. Commun.* **2014**, *40*, 108 – 111.

[20] a) Z.-M. Zhang, S. Yao, Y.-G. Li, Y.-H. Wang, Y.-F. Qi, E.-B. Wang, *Chem. Commun.* **2008**, 1650 – 1652; b) S. Yao, Z.-M. Zhang, Y.-G. Li, E.-B. Wang, *Dalton Trans.* **2010**, *39*, 3884 – 3889.

[21] a) B. Godin, Y. Chen, J. Vaissermann, L. Ruhlmann, M. Verdaguer, P. Gouzerh, *Angew. Chem. Int. Ed.* **2005**, *44*, 3072 – 3075; *Angew. Chem.* **2005**, *117*, 3132 – 3135; b) F. Hussain, U. Kortz, B. Keita, L. Nadjo, M. T. Pope, *Inorg. Chem.* **2006**, *45*, 761 – 766.

[22] X. Fang, P. Kögerler, *Angew. Chem. Int. Ed.* **2008**, *47*, 8123 – 8126; *Angew. Chem.* **2008**, *120*, 8243 – 8246.

[23] a) S. Mukherjee, J. A. Stull, J. Yano, T. C. Stamatatos, K. Pringouri, T. A. Stich, K. A. Abboud, R. D. Britt, V. K. Yachandra, G. Christou, *Proc. Natl. Acad. Sci. USA* **2012**, *109*, 2257 – 2262; b) T. N. Nguyen, M. Shiddiq, T. Ghosh, K. A. Abboud, S. Hill, G. Christou, *J. Am. Chem. Soc.* **2015**, *137*, 7160 – 7168.

[24] N. F. Chilton, R. P. Anderson, L. D. Turner, A. Soncini, K. S. Murray, *J. Comput. Chem.* **2013**, *34*, 1164 – 1175.

[25] a) K. S. Cole, R. H. Cole, *J. Chem. Phys.* **1941**, *9*, 341 – 351; b) S. M. Aubin, Z. Sun, L. Pardi, J. Krzysteck, K. Folting, L.-J. Brunel, A. L. Rheingold, G. Christou, D. N. Hendrickson, *Inorg. Chem.* **1999**, *38*, 5329 – 5340.

[26] a) M. Filowitz, R. K. C. Ho, W. G. Klemperer, W. Shum, *Inorg. Chem.* **1979**, *18*, 93 – 103; b) R. Contant, *Inorg. Synth.* **1990**, *27*, 104 – 111.

[27] a) G. Sheldrick, *Acta Crystallogr. Sect. A* **1990**, *46*, 467 – 473; b) G. Sheldrick, *Acta Crystallogr. Sect. A* **2008**, *64*, 112 – 122.

Received: July 23, 2015